

# Multiwavelength Observations of a Dramatic High Energy Flare in the Blazar 3C 279

A. E. Wehrle<sup>1</sup>, E. Pian<sup>2,3</sup>, C. M. Urry<sup>2</sup>, L. Maraschi<sup>4</sup>, G. Ghisellini<sup>5</sup>, R. C. Hartman<sup>6</sup>, G. M. Madejski<sup>6</sup>, F. Makino<sup>7</sup>, A. P. Marscher<sup>8</sup>, I. M. McHardy<sup>9</sup>, S. J. Wagner<sup>10</sup>, J. R. Webb<sup>11,12</sup>, G. S. Aldering<sup>13</sup>, M. F. Aller<sup>14</sup>, H. D. Aller<sup>14</sup>, D. E. Backman<sup>15</sup>, T. J. Balonek<sup>16</sup>, P. Boltwood<sup>17</sup>, J. Bonnell<sup>6</sup>, J. Caplinger<sup>6</sup>, A. Celotti<sup>18</sup>, W. Collmar<sup>19</sup>, J. Dalton<sup>15</sup>, A. Drucker<sup>15</sup>, R. Falomo<sup>20</sup>, C. E. Fichtel<sup>6</sup>, W. Freudling<sup>21</sup>, W. K. Gear<sup>22</sup>, N. Gonzalez-Perez<sup>23</sup>, P. Hall<sup>24</sup>, H. Inoue<sup>7</sup>, W. N. Johnson<sup>25</sup>, D. Kazanas<sup>6</sup>, M. R. Kidger<sup>23</sup>, T. Kii<sup>7</sup>, R. I. Kollgaard<sup>26</sup>, Y. Kondo<sup>6</sup>, J. Kurfess<sup>25</sup>, A. J. Lawson<sup>9</sup>, Y. C. Lin<sup>27</sup>, B. McCollum<sup>6</sup>, K. McNaron-Brown<sup>25</sup>, F. Nagase<sup>7</sup>, A. D. Nair<sup>28</sup>, S. Penton<sup>29</sup>, J. E. Pesce<sup>2,30</sup>, M. Pohl<sup>19</sup>, C. M. Raiteri<sup>31</sup>, M. Renda<sup>15</sup>, E. I. Robson<sup>22,32</sup>, R. M. Sambruna<sup>6,30</sup>, A. F. Schirmer<sup>16</sup>, C. Shrader<sup>6</sup>, M. Sikora<sup>33</sup>, A. Sillanpää<sup>34</sup>, P. S. Smith<sup>35</sup>, J. A. Stevens<sup>32</sup>, J. Stocke<sup>29</sup>, L. O. Takalo<sup>34</sup>, H. Teräsranta<sup>36</sup>, D. J. Thompson<sup>6</sup>, R. Thompson<sup>6</sup>, M. Tornikoski<sup>36</sup>, G. Tosti<sup>37</sup>, P. Turcotte<sup>15</sup>, A. Treves<sup>38</sup>, S. C. Unwin<sup>39</sup>, E. Valtaoja<sup>36</sup>, M. Villata<sup>31</sup>, W. Xu<sup>1</sup>, A. Yamashita<sup>7</sup>, A. Zook<sup>40</sup>

---

<sup>1</sup>Infrared Processing Analysis Center, MC 100-22, Jet Propulsion Laboratory and California Institute of Technology, Pasadena, CA 91125

<sup>2</sup>Space Telescope Science Institute, 3700 San Martin Drive, Baltimore, MD 21218

<sup>3</sup>ITESRE-CNR, Via Gobetti 101, I-40129 Bologna, Italy

<sup>4</sup>Osservatorio Astronomico di Brera, Via Brera 28, I-20121 Milan, Italy

<sup>5</sup>Osservatorio Astronomico di Brera, Via Bianchi 46, I-22055 Merate (Lecco), Italy

<sup>6</sup>NASA/Goddard Space Flight Center, Greenbelt, MD 20771

<sup>7</sup>ISAS, 3-1-1, Yoshinodai, Sagamihara, Kanagawa 229, Japan

<sup>8</sup>Department of Astronomy, Boston University, 725 Commonwealth Avenue, Boston, MA 02215

<sup>9</sup>Department of Physics, University of Southampton, Southampton SO9 5NH, United Kingdom

<sup>10</sup>Landessternwarte, Heidelberg-Königsstuhl, D-69117 Heidelberg, Germany

<sup>11</sup>Department of Physics, Florida International University, University Park, Miami, FL 33199

<sup>12</sup>SARA Observatory, KPNO/NOAO, 950 North Cherry Avenue, P.O. Box 26732, Tucson, AZ 85726

<sup>13</sup>University of Minnesota, Department of Astronomy, 116 Church St., SE Minneapolis, MN 55455

<sup>14</sup>University of Michigan, Physics and Astronomy, 817 Dennison Building, Ann Arbor, MI 48109

<sup>15</sup>Franklin & Marshall College, Physics & Astronomy Department, P.O. Box 3003, Lancaster, PA 17604-3003

<sup>16</sup>Colgate University, Department of Physics & Astronomy, 13 Oak Dr., Hamilton, NY 13346-1398

<sup>17</sup>1655 Main St., Stittsville, Ontario, Canada K2S 1N6

<sup>18</sup>SISSA/ISAS, Via Beirut 2-4, I-34014 Miramare-Grignano (Trieste), Italy

<sup>19</sup>Max Planck-Institut für Extraterrestrische Physik, Giessenbachstrasse, D-85740 Garching bei München, Germany

<sup>20</sup>Osservatorio Astronomico di Padova, Via Osservatorio 5, I-35122 Padova, Italy

<sup>21</sup>Space Telescope European Coordinating Facility, Karl-Schwarzschild Strasse 2, D-85748 Garching bei München, Germany

<sup>22</sup>Centre for Astrophysics, University of Central Lancashire, Preston, PR1 2HE, United Kingdom

<sup>23</sup>Instituto de Astrofísica de Canarias, E-38200, La Laguna, Tenerife, Spain

<sup>24</sup>Steward Observatory, University of Arizona, Tucson AZ 85721

<sup>25</sup>Naval Research Lab., 4555 Overlook Av., SW Washington, DC 20375-5352

<sup>26</sup>Fermi National Accelerator Laboratory, Kirk Road and Pine Street, Batavia, IL 60510

<sup>27</sup>W. W. Hansen Experimental Physics Laboratory and Department of Physics, Stanford University,

## ABSTRACT

The blazar 3C 279, one of the brightest identified extragalactic objects in the  $\gamma$ -ray sky, underwent a large (factor of  $\sim 10$  in amplitude) flare in  $\gamma$ -rays towards the end of a 3-week pointing by CGRO, in 1996 January-February. The flare peak represents the highest  $\gamma$ -ray intensity ever recorded for this object. During the high state, extremely rapid  $\gamma$ -ray variability was seen, including an increase of a factor of 2.6 in  $\sim 8$  hr, which strengthens the case for relativistic beaming. Coordinated multifrequency observations were carried out with RXTE, ASCA, ROSAT and IUE and from many ground-based observatories, covering most accessible wavelengths. The well-sampled, simultaneous RXTE light curve shows an outburst of lower amplitude (factor of  $\simeq 3$ ) well correlated with the  $\gamma$ -ray flare without any lag larger than the temporal resolution of  $\sim 1$  day. The optical-UV light curves, which are not well sampled during the high energy flare, exhibit more modest variations (factor of  $\sim 2$ ) and a lower degree of correlation. The flux at millimetric wavelengths was near an historical maximum during the  $\gamma$ -ray flare peak and there is a suggestion of a correlated decay. We present simultaneous spectral energy distributions of 3C 279 prior to and near to the flare peak. The  $\gamma$ -rays vary by more than the square of the observed IR-optical

---

Stanford, CA 94305

<sup>28</sup>Department of Astronomy, University of Florida, Gainesville, FL 32601

<sup>29</sup>University of Colorado, JILA, Campus Box 440, Boulder, CO 80309-0440

<sup>30</sup>Pennsylvania State University, Dept. of Astronomy, 525 Davey Lab, University Park, PA 16802

<sup>31</sup>Osservatorio Astronomico di Torino, Strada Osservatorio 20, I-10025 Pino Torinese, Italy

<sup>32</sup>Joint Astronomy Centre, 660 N. Aohoku Place, University Park, Hilo, HI 96720

<sup>33</sup>Copernicus Astronomical Center, Polish Academy of Science, Warsaw, Poland

<sup>34</sup>Tuorla Observatory, Tuorla 21500 Piikkiö, Finland

<sup>35</sup>NOAO/KPNO, N. Cherry Avenue, P.O. Box 26732, Tucson, AZ 85726

<sup>36</sup>Metsähovi Radio Research Station, 02540 Kylmälä, Finland

<sup>37</sup>Osservatorio Astronomico, Università di Perugia, I-06100 Perugia, Italy

<sup>38</sup>Department of Physics, University of Milan at Como, Via Lucini 3, I-22100 Como, Italy

<sup>39</sup>MS 306-388, Jet Propulsion Laboratory, California Institute of Technology, 4800 Oak Grove Drive, Pasadena, CA 91109

<sup>40</sup>Pomona College, Department of Physics & Astronomy, 610 College Ave., Claremont, CA 91711-6359

flux change, which poses some problems for specific blazar emission models. The synchrotron- self Compton model would require that the largest synchrotron variability occurred in the mostly unobserved sub-mm/far-infrared region. Alternatively, a large variation in the external photon field could occur over a time scale of few days. This occurs naturally in the “mirror” model, wherein the flaring region in the jet photoionizes nearby broad-emission-line clouds, which in turn provide soft external photons that are Comptonized to  $\gamma$ -ray energies.

*Subject headings:* Galaxies: active — gamma rays: observations — quasars: (3C 279) — radiation mechanisms: non-thermal

## 1. Introduction

The remarkable emission of blazars in the MeV-GeV energy range, relativistically enhanced by Doppler beaming, has made them the only class of Active Galactic Nuclei detected by the EGRET instrument on CGRO (Thompson et al. 1995). The quasar 3C 279 ( $z = 0.538$ ), the first radio source in which superluminal motion was discovered, is a prototype of the blazar class. It is the second brightest  $\gamma$ -ray blazar (Kniffen et al. 1993), the brightest being PKS 1622-297; (Mattox et al. 1997).

Violent variability is a distinguishing property of blazars and the  $\gamma$ -ray emission is no exception, varying with large amplitude on time scales of days or less (see recent review by Hartman 1996), implying a very compact emission region. The radio to UV continuum from blazars is commonly interpreted as synchrotron radiation from high energy electrons in a relativistic jet, while the MeV-GeV photons are believed to be emitted via inverse Compton scattering of soft seed photons by the same electrons (e.g., Ulrich, Maraschi, & Urry 1997). Finding correlations among the variations at high (X- to  $\gamma$ -ray) and low frequencies is therefore critical to understanding which ranges of the Compton and synchrotron components are due to the same electrons and to clarify the nature of the seed photons available for scattering, namely whether they are generated within the jet (synchrotron-self Compton, SSC) or in regions external to the jet, like the accretion disk or the broad-emission-line clouds (external Compton, EC).

Multiwavelength observations of blazars in conjunction with EGRET pointings have been obtained at several epochs. However, either the monitoring was too sparse or the source was not active during the campaign, so that detections of correlated multiwavelength variability on short time scales are tentative (3C 279, Maraschi et al. 1994; Hartman et al. 1996; OJ 287, Webb et al. 1996; PKS 0537-441, Pian et al. 1997). A comparison of

the spectral energy distribution of 3C 279 during the historically brightest state of the source (1991 June) with the lowest state ever observed (1992 December - 1993 January) showed that the  $\gamma$ -ray flux variation between the two epochs was larger than at any other wavelength (Maraschi et al. 1994), as predicted qualitatively by the SSC model (Maraschi, Ghisellini, & Celotti 1992). Multiwavelength variability between 1991 June and October was found to follow the same behavior (Hartman et al. 1996). The larger  $\gamma$ -ray variability could also be accommodated within an EC scenario provided there was a change in the bulk Lorentz factor of the  $\gamma$ -ray emitting plasma, or the external photon field varied for some other reason, possibly as a result of enhanced photoionization of surrounding broad-line clouds by the jet itself.

The multiwavelength campaign on 3C 279 in 1996 January-February was organized as a 2-week coordinated program of the CGRO, ROSAT, RXTE and IUE spacecraft, plus a 1-week Target of Opportunity extension triggered by the high intensity measured with EGRET during the first week. The aim was to follow the evolution of a short-time-scale outburst at all frequencies, in order to constrain the possibility of a variation of the bulk Lorentz factor. This would allow discriminating between the possible models, and clarifying the nature of the seed photons being inverse Compton-scattered to  $\gamma$ -ray energies. The campaign also benefitted from the simultaneous and quasi-simultaneous observations with the HST, ASCA, and ISO satellites, as well as with many ground-based radio and optical telescopes. The final data set is rich in both temporal and wavelength coverage to an extent unmatched by any other blazar. In this paper we present the observations conducted at the radio-to- $\gamma$ -ray facilities participating in the multiwavelength monitoring (§ 2), the light curves obtained (§ 3), and the spectral energy distributions before and near the flare peak (§ 4). We then compare our results with those at previous epochs and discuss constraints on theoretical models (§ 5) and summarize our findings (§ 6).

## 2. Observations

In the following we give the essential information on the observations at each wavelength and summarize the results in Table 1. The multiwavelength light curves of 3C 279 from 1996 January 11 through 1996 February 13 are shown in Figure 1 on a logarithmic scale. Included are data with the most complete temporal coverage and at the full range of wavelengths. We defer to separate papers for a complete presentation and for details about data analysis. In particular, a complete account of the  $\gamma$ -, X-ray and ISO observations, data reduction and analysis will be given in Hartman et al. (1997), McHardy et al. (1997), and Barr et al. (1997), respectively.

During the CGRO observations from 1996 January 16-30, 3C 279 was close to the center of the field of view of EGRET and COMPTEL (5.0-6.7 deg). OSSE began observations on 1996 January 24. Due to the outstanding brightness detected by EGRET, the pointing was extended through 1996 February 6 as part of a Target of Opportunity program. The high emission state of 3C 279 made it possible to detect significant signal with EGRET for integration times of 1 day, and even of 8 hours during the flare. The light curves are shown in Figure 1a. Analysis of the EGRET spectrum during the flare, from February 4-6, yielded an energy index  $\alpha_\nu = 0.97 \pm 0.07$  between 30 MeV and 10 GeV, and  $\alpha_\nu = 1.07 \pm 0.09$  was found for the period January 16-30. We use the convention  $f_\nu \propto \nu^{-\alpha_\nu}$ . COMPTEL detected the source at energies above 3 MeV. Over the whole period the average flux in the 10-30 MeV band was  $(2.6 \pm 0.6) \times 10^{-5}$  photons  $\text{s}^{-1} \text{cm}^{-2}$ . The average energy spectrum tends to be hard ( $\alpha_\nu < 1$ ), however, the power-law slope cannot be determined accurately due to non-detection below 3 MeV. The source was in the OSSE field of view from January 24 to February 7, and was detected in each of the two weeks at a high confidence level.

The RXTE satellite began observing 3C 279 less than a month after launch and monitored the source for 20 minutes daily from January 21 to February 10 during its performance verification phase (McHardy et al. 1997), preceded by 6 days of observations with the ROSAT-HRI (January 14-20) and accompanied by one 20-kilosecond ASCA pointing on January 27 (Makino et al. 1996). The RXTE data were calibrated by performing background subtraction from slewing data; the ASCA spectral index  $\alpha_\nu = 0.7$  was used to calculate flux densities. The robustness of the RXTE background modelling is demonstrated by the agreement of the flux densities at the low end of the RXTE energy range and the high end of the ROSAT energy range on the day(s) in which their coverage overlapped. The X-ray light curve is shown in Figure 1b.

IUE observed 3C 279 at approximately daily intervals from January 15.6 to February 6.8 with the LWP camera and on one occasion (January 25) with the SWP. The 13 LWP spectra were reduced and calibrated according to the Final Archive processing routine which adopts the NEWSIPS method for spectral extraction (Nichols & Linsky 1996). Ly $\alpha$  emission (1216 Å) is clearly visible on the SWP spectrum redshifted to  $\sim 1870$  Å with a dereddened intensity of  $(5 \pm 2) \times 10^{-14}$  erg  $\text{s}^{-1} \text{cm}^{-2}$ . No emission line is present in the LWP spectra. The LWP spectral signal was integrated and averaged in the 2500-2700 Å interval, where the camera sensitivity is highest and the solar scattered light contamination (which might have been present in the first half of the monitoring) is negligible. The SWP signal was averaged in the 1400-1600 Å range, where the camera sensitivity is high and no emission lines are superposed on the continuum. Uncertainties are computed as in Falomo et al. (1993). The LWP light curve is shown in Figure 1c.

The source was observed with the HST Faint Object Spectrograph using the G130H and G190H gratings, exposed for 2820 and 2250 seconds, respectively, just before the start of the multifrequency campaign on 1996 January 8 as part of a different program whose results will be reported elsewhere (Stocke et al. 1997). The shape of the dereddened spectral flux distribution in the interval 1300-2240 Å is described by a power-law with energy index  $\alpha_\nu = 1.81 \pm 0.05$ . Although not obtained during the EGRET pointing, these data are of interest here since they yield a reliable measure of the Ly $\alpha$  intensity which is important in estimating the inverse Compton contribution from external seed photons. The dereddened line intensity is  $(4 \pm 1) \times 10^{-14} \text{ erg s}^{-1} \text{ cm}^{-2}$ .

Optical BVRI photometry was obtained at several different sites listed in Table 2. The R-band has the best temporal coverage including one point close to the peak of the  $\gamma$ -ray flare, so only those data are shown in Figure 1d. The data in the B-band are very sparse; those in V- and I-bands show the same behavior as the R-band light curve within the uncertainties. The conversion of optical magnitudes to fluxes has been done following Bessel (1979). For a presentation of the complete data set of ground-based optical, near-IR, millimeter and radio observations, as well as for the IUE data related to this campaign, we defer to a separate paper. The near-IR emission of 3C 279 was measured in the J, H and K bands at CTIO on January 31 and February 3. Only two data points were obtained within the time span of the campaign for each filter (Table 1). The conversion from JHK magnitudes to fluxes follows Bersanelli, Bouchet, and Falomo (1991).

The source was observed at millimeter and sub-millimeter wavelengths at the JCMT with both heterodyne and bolometer receivers as part of an extensive campaign that lasted through 1996 June. Few observations were obtained during the campaign reported here, but they were close in time to the  $\gamma$ -ray peak. The 0.45- and 0.8-mm data are shown in Figure 1e. At longer wavelengths the variations were smaller. Bolometric observations at millimeter wavelengths were carried out with the 30m IRAM telescope using the IRAM/MPI 7-channel bolometer on 1996 January 13. The nominal frequency of the bolometer is 250 GHz, the bandwidth about 60 GHz. The observations were carried out under poor weather conditions. Observations of Uranus in the same night after weather conditions significantly improved were used for the flux calibration, assuming a flux of 35.18 Jy. The standard recommended gain-elevation correction was applied. The resulting fluxes of the two observations were  $(33.7 \pm 0.3) \text{ Jy}$  and  $(18.2 \pm 1.1) \text{ Jy}$ , where the errors are the rms of the single scans within each observations. We attribute the difference in the results to the changing weather conditions, and adopt a value of  $(26 \pm 8) \text{ Jy}$ .

Radio observations at 37 and 22 GHz were conducted at the Metsähovi Radio Research Station from January 3 to February 11 and at 4.8, 8 and 14.5 GHz from January 2 to

March 1, altogether, at the University of Michigan Radio Astronomical Observatory, as part of longterm monitoring programs. The resulting light curves at the three highest radio frequencies are shown in Figure 1f.

### 3. Comparison of Multiwavelength Light Curves

The 1-day binned EGRET light curve shows an extraordinary flare peaking on February 5 (Fig. 1a). Before January 30, the fluctuations visible to the eye in the  $\gamma$ -ray light curve are probably not due to real variability (the probability of variability is 30%, according to a  $\chi^2$  test). The peak flux represents an increase by a factor of 10 with respect to the average level between January 20 and 30. The 8-hour binned EGRET light curve during the outburst appears modulated by high amplitude variations, the largest of which, a factor of 4-5 in one day, has a doubling time of only  $\tau_D = 6$  hours ( $\tau_D \equiv \frac{F_{initial}}{\Delta F} \cdot \Delta t$ ). Between the January 16-30 and the Target-of-Opportunity periods, the flux in the 10-30 MeV range (COMPTEL) increased by a factor of 3.6 ( $2.5\sigma$  significance level). No significant variability on timescales of days was found in the OSSE data, according to a  $\chi^2$  test.

The X-ray light curve also shows a large outburst, well correlated in time with the  $\gamma$ -ray flare but of lower amplitude (factor of 3, Fig. 1b). Any possible lag is less than the temporal resolution of 1 day, as confirmed by an analysis with the Discrete Correlation Function method (DCF, Edelson & Krolik 1988). The width of the outburst is about 7 days in X-rays, where the data extend from the pre-flare state to the decay, while the  $\gamma$ -ray coverage ends one day after the flare peak. The ROSAT HRI data did not reveal any variability larger than 10%, therefore the average 1 keV flux has been reported here as well as for the ASCA observation.

The light curve at 2600 Å (IUE-LWP) is reasonably well-sampled during the first part of the campaign but not toward the end, when the  $\gamma$ -ray flare occurred (Fig. 1c). It shows a broad minimum at  $\sim$  January 25-26 followed by a rise of almost a factor of 2, but with a three-day gap before and up to the  $\gamma$ -ray peak. If the UV minimum were associated with the (possible) minimum in the EGRET light curve at January 28, this would indicate a correlation with the UV leading the  $\gamma$ -rays by  $\sim 2.5$  days. In this case the UV maximum would have occurred before the  $\gamma$ -ray peak, during the gap in IUE monitoring between February 1 and 5. Unfortunately, the UV and  $\gamma$ -ray light curves have too few points to apply the DCF method efficiently, so no robust result can be found from their cross-correlation.

The R-band light curve is similar to the UV light curve in showing a broad minimum

on days January 26-28 followed by a rise (Fig. 1d). Again, the sampling around the  $\gamma$ -ray flare is very poor. One observation very close to the flare peak yields a flux higher than the average around day January 28 by a factor of 1.6. The behavior in V and I (not shown) is similar. On the whole, the optical light curves suggest that the minimum occurs later than the UV minimum by 1-2 days. They resemble the  $\gamma$ - and X-ray light curves in the flare rise, but differ significantly in having values quite close to those at the peak also at other epochs (e.g., around January 20) when the high energy light curves have values much lower than the peak. In other words, the flare stands out in the high energy light curves while it is not apparent as such in the UV-optical light curves. A near-infrared flux increase was observed, whose amplitude is a factor of 1.3 in J and H, and 1.2 in K band. Therefore, within the limited sampling, the JHK data are consistent with the rising trend of the other light curves.

The submillimeter data are rather sparse, but show variability consistent with the occurrence of a flare around February 3 (Fig. 1e). The sparse sampling prevents us from determining conclusively that the submillimeter peak actually occurred on February 3; it could as well have occurred on January 30, 31 or February 1, 2. Observations at 0.45, 0.8, 1.1, 1.3 and 2 mm on February 5 and 6 show a decline in flux, of decreasing amplitude with increasing wavelength, corresponding to the  $\gamma$ - and X-ray decline after the outburst. We notice that the level of the mm/sub-mm flux reached during the present campaign has been exceeded only once (in 1994) in the last 7 years, and in 1996 May a further increase by 20-30% was recorded.

At radio frequencies the variability is highly significant (Fig. 1f). There is a nearly monotonic increase of  $\lesssim 30\%$  amplitude at 37 GHz from January 18 to February 9, and a smaller increase at lower frequencies. A 6-7 Jy rise in 20 days is rare in the 16-year Metsähovi database. The brightness reached its historic maximum (since 1980) during May-June 1996, a time delay of about 4 months relative to the X- and  $\gamma$ -ray flare.

#### 4. Radio-to- $\gamma$ -ray Energy Distributions

The multiwavelength data collected during the 1996 monitoring campaign allow us to follow the evolution of the overall spectrum of 3C 279 from a quasi-stationary state through the development of a dramatic high-energy outburst. There is no unique definition of a pre-flare state. In Figures 2 and 3 we show average fluxes in the period January 24-28 (where available), which includes the UV and optical minima. The epoch of the high energy outburst is well covered at most wavelengths, no more than 2 days from the  $\gamma$ -ray peak. We can therefore construct a reliable spectral energy distribution (SED) for the highest state.

We averaged the available data in a 2-day window centered on the  $\gamma$ -ray peak (February 4-6). The resulting SED for the flaring state is shown in Figures 2 and 3. Near-IR, optical and UV data (Table 1) have been corrected (shown in Figures 2 and 3) according to Cardelli, Clayton and Mathis (1989) for Galactic interstellar extinction using  $N_H = 2.22 \times 10^{20}$   $\text{cm}^{-2}$  (Elvis et al. 1989), a gas-to-dust ratio  $N_H/E_{B-V} = 5.2 \times 10^{21}$   $\text{cm}^{-2}$   $\text{mag}^{-1}$  (Shull & Van Steenberg 1985), and a total-to-selective extinction ratio  $A_V/E_{B-V} = 3.1$  (Rieke & Lebofsky 1985). The X-ray count rates have been converted to flux units using a power-law energy index of 0.7 derived from the ASCA 2-10 keV observations. The  $\gamma$ -ray photon counts have been converted to fluxes at 0.4 GeV according to Thompson et al. (1996).

The spectrum consists of two broad humps with peaks at  $\sim 10^{12} - 10^{13}$  Hz and  $10^{22} - 10^{24}$  Hz. ISO data (Barr et al. 1997) will be of great importance to determine the shape of the SED in the range where the maximum synchrotron power is expected to be emitted. It is interesting to note that the sub-millimeter spectral slope during the flare ( $\alpha_\nu = 0.38 \pm 0.09$  on February 5 and  $\alpha_\nu = 0.51 \pm 0.08$  on February 6) is roughly the same as the hard-X-ray to MeV- $\gamma$ -ray spectrum ( $\alpha_\nu \sim 0.6$ ), as expected if the same electrons are responsible for the synchrotron and inverse Compton-scattered radiation at those energies. Comparing the flare and pre-flare states it is clear that the high energy spectrum (X- to  $\gamma$ -rays) is harder at the flare peak, as implied by the larger amplitude of the  $\gamma$ -ray variation. From near-IR to UV frequencies the flare versus pre-flare variations are smaller than in X- and  $\gamma$ -rays. Comparing simultaneous J, H and K fluxes at two epochs suggests again that the variability amplitude increases with frequency, but the effect does not show up comparing UV to V, R or I band variations. There is little information on the pre-flare fluxes at still lower frequencies, except for the radio band which is only weakly coupled to the rest of the SED. We note, however, that from the few data points available the amplitude of the variations at 0.45 and 0.8 mm is comparable to that of the simultaneous X-ray variations.

The SEDs of 3C 279 obtained during the 1991 June high state and the 1993 January low state are also shown in Figure 3 for comparison with the flare and pre-flare SEDs derived here. The 1991  $\gamma$ -ray data are averaged over the 2-week pointing which included the flare. The X-ray and R band observations were simultaneous, while the other measurements were close in time except for the UV spectrum which was obtained one month later (Hartman et al. 1996).

## 5. Discussion

In early 1996, the blazar 3C 279 was observed in its highest  $\gamma$ -ray emission state ever. The pre-flare flux level (before 1996 February 1) was comparable to the average state in 1991 June (Kniffen et al. 1993; Hartman et al. 1996). The presently observed maximum exceeds by a factor of  $\sim 3$  the peak of the 1991 June 24–25 outburst, the brightest state recorded previously, and is  $\sim 90$  times higher than the historical  $\gamma$ -ray minimum seen with EGRET in 1992 December–1993 January (Maraschi et al. 1994). Inspection of Figure 1 indicates decreasing variability amplitude with decreasing energy (within either the synchrotron or inverse Compton component), which is a common characteristic of blazar variability (e.g., 3C 279 itself, Maraschi et al. 1994; PKS 2155–304, Urry et al. 1997). In addition, the X-ray emission during the 1996 outburst was higher than measured in 1991 June with *Ginga* over approximately the same energy range (Fig. 2). Thus, not only is the X-ray variability amplitude lower than the  $\gamma$ -ray during the 1996 flare, but over longer time-scales the overall amplitude is also lower. Notice that the flaring multiwavelength SED in 1996 February presents an “inverted” variation with respect to the 1991 state: while the  $\gamma$ -ray flux is *higher* than in 1991 by a factor of  $\sim 4$  and the optical-UV flux is *lower* than earlier by a factor of  $\sim 1.5$ -2.

During the 1996 observations, significant  $\gamma$ -ray variability was found on time scales comparable to the sampling resolution (i.e., 8 hours). Such extremely fast variability has also been found in several other blazars (Hartman 1996; Mattox et al. 1997). The amplitude and rapidity of these luminosity changes exceed a well-known limit based on accretion efficiency (Fabian 1979; Dermer & Gehrels 1995), which probably occurs in blazars because their observed radiation comes from relativistically beamed jets (with unknown relation to accretion processes). The simultaneous variability in X- and GeV  $\gamma$ -rays shows for the first time that they are approximately co-spatial. This, plus the rapid  $\gamma$ -ray variability, gives a strong lower limit to the beaming factor from the condition that the emission region should be transparent to  $\gamma$ -rays ( $\tau_{\gamma\gamma} \propto \delta^{-5} L / \Delta t$ ). For the optical depth to photon-photon absorption to be less than unity, the required beaming factor is  $\delta_\gamma \geq 6.3$  or  $\delta_\gamma \geq 8.5$  for photons of  $\sim 1$  or  $\sim 10$  GeV, respectively. These values are derived following Dondi and Ghisellini (1995), but are somewhat larger than theirs due to the faster variability now observed. An independent argument for relativistic bulk motion of the low-frequency emitting region comes from the limit to the X-ray flux produced by the self-Compton process (Marscher et al. 1979), which gives  $\delta \geq 18$  (Ghisellini et al. 1993). A third estimate comes from the observed superluminal expansion of VLBI-resolved knots,  $\delta \sim 6$  (preliminary estimate from Wehrle et al. 1997).

In low-frequency peaked blazars like 3C 279, high energy electrons in a relativistic jet

radiate at radio through UV wavelengths via the synchrotron process, and can produce X- and  $\gamma$ -rays by scattering soft target photons present either in the jet (SSC) or in the surrounding ambient (EC, Maraschi, Ghisellini, & Celotti 1992; Blandford 1993; Dermer, Schlickeiser, & Mastichiadis 1992; Sikora, Begelman, & Rees 1994). The relative variability in the synchrotron and inverse Compton components can indicate the origin of these seed photons. Specific, time dependent models are clearly necessary for an in depth discussion but are beyond the scope of this paper. In the following we discuss in general terms different scenarios for the origin of the seed photons assuming that a single active blob in the jet is responsible for the variability.

The SSC model predicts that a change in the electron spectrum (intensity and/or shape) should cause larger variability in the inverse Compton emission than in the synchrotron emission because the energy densities of the seed photons and the scattering electrons vary in phase. In a one-zone model, the peak flux of the inverse Compton SED should vary approximately quadratically with the peak flux of the synchrotron distribution (Ghisellini & Maraschi 1996). Between 1991 June and 1993 January this quadratic variation condition was satisfied assuming the synchrotron peak was close to the IR band (Maraschi et al. 1994; Ghisellini & Maraschi 1996), but for the 1996 flare vs. pre-flare SEDs the amplitude of the  $\gamma$ -ray variation is *more than the square* of the IR-optical-UV flux variation. However, there are very few data close to the  $\gamma$ -ray maximum (the IR points are from February 3, which is at half maximum), and the synchrotron peak may also fall at lower frequencies ( $\sim 10^{13}$  Hz, as suggested by the strong flux at millimetric wavelengths) where adequate variations could have occurred. A further caveat is that different emission zones could contribute to the IR-optical flux, diluting the intrinsic variation due to the  $\gamma$ -ray emitting region. We conclude that the SSC scenario can not be ruled out by the present data.

Alternatively, we consider the EC scenario, (Sikora, Begelman, and Rees 1994) where the seed photons are external to the jet and independent of it. In this case: (i) the inverse Compton emission should vary linearly with the synchrotron emission for changes in the electron spectrum; and (ii) larger than linear variations of the inverse Compton emission can be explained if the bulk Lorentz factor of the emission region varies together with the electron spectrum. In the latter case the different beaming patterns of synchrotron and inverse Compton radiation should also be taken into account (Dermer 1995). As for the SSC model, different emission zones contributing to the IR- optical flux would dilute the intrinsic variation due to the  $\gamma$ -ray emitting region. While the second case is conceivable comparing SEDs separated by years, it is far less likely that the entire emission region could accelerate *and decelerate* significantly over the time-scale of the rapid flare observed here. The first case is unlikely because of the apparent nonlinear response of the  $\gamma$ -rays to the

synchrotron variability.

An interesting alternative combining advantages of both the SSC and EC scenarios is the “mirror” model of Ghisellini & Madau (1996). Here the seed photons are provided by rapidly varying broad-line emission from a few clouds close to the jet and photoionized by an active blob in it. First, the photoionizing continuum is beamed and therefore intense and highly variable; second, the electrons in the jet see broad-line emission from the nearest cloud(s) as beamed; and, third, the  $\gamma$ -ray emitting blob, approaching the clouds, will see an increasing radiation energy density due to the decreasing blob-cloud distance. These effects lead to a more-than-quadratic increase in  $\gamma$ -rays associated with variations in synchrotron emission from the active blob. This picture requires rather special conditions in that the cloud(s) close to the jet must also have a large covering factor, to let their emission line flux dominate the radiation energy density seen by the blob. The observations presented here can be accounted for by the mirror model if the far-UV (photoionizing) emission varied during the flare by a factor of 3-4. This was not directly observed but is consistent with an extrapolation from the UV variations. If an increase occurred as an active region of the jet approached one or more broad-line clouds lying within the jet’s beam, the observed amplitude of  $\gamma$ -ray variability could be explained, at least qualitatively. Also, the asymmetric shape of the X-ray curve, in which the decay is possibly faster than the rise, can be accommodated by the mirror model since the inverse Compton emission drops sharply (because of the narrow angular pattern of the beaming) once the active part of the jet passes the broad line cloud(s).

We note that no variations in the Ly $\alpha$  luminosity are seen in archival (IUE and HST) spectra of 3C 279, as opposed to a large historical variability of the continuum, implying that a steady component, like an accretion disk, rather than the jet beam, dominates the overall photoionization of the broad line clouds (Koratkar et al. 1997). However the jet could still play a significant role in powering the clouds close to it. The mirror model could be tested in principle, even in the absence of any available  $\gamma$ -ray observations, by monitoring the Ly $\alpha$  emission line of 3C 279. A limited number of clouds, over a limited velocity range, should respond simultaneously to the most rapidly varying (time scales of days) jet emission. However, the observed variability amplitude may be small, being diluted by the overall broad line region emission. The line intensity measurements of January 8 and 25 from the HST-FOS and IUE-SWP spectra respectively, indicating no change, are inconclusive because they both refer to the pre-flare epoch and to similar continuum levels. Moreover the IUE sensitivity is far too low to measure variations in the line profile.

## 6. Summary

Radio-to- $\gamma$ -ray monitoring of the blazar 3C 279 in 1996 January-February recorded the highest  $\gamma$ -ray flux of the source ever measured. A correlated flare at X- and  $\gamma$ -ray energies with an amplitude of a factor 3 and 10, respectively, is seen and completely resolved. The data at optical and UV frequencies clearly show a flux increase correlated with the X- and  $\gamma$ -ray rise, although the poor sampling close to the flare peak prevents a precise measurement of the amplitude in these bands. The millimetric flux measured only close to the flare peak shows variability which could be correlated with the high energy light curves. The radio emission exhibited variations of remarkable rapidity and amplitude. The relative amplitudes of the high energy and low energy light curves during the flare and the apparently stronger IR to UV emission in 1991 June, when the average  $\gamma$ -ray flux was weaker, represent important challenges for our understanding of blazars. The data do not rule out SSC models especially if more than one zone contributes to the emission, but are difficult to reconcile with a scenario in which the seed photons are provided by the ambient surrounding the jet and independent from it. A picture in which the relativistic jet hits and ionizes a small fraction of the broad line clouds which then provide the photons to be inverse-Compton upscattered seems appealing and likely. Sensitive measurements of variations in the profile of the strong Ly $\alpha$  line correlated with the beamed UV continuum could test this model.

We are grateful to the staffs of ISO, IUE, HST, ASCA, ROSAT, XTE, CGRO, CTIO, JCMT, IRAM, IAC Tenerife, Metsähovi Station, UMRAO, NURO, Lowell Observatory, Boltwood Observatory, Foggy Bottom Observatory, the Burrell Schmidt Observatory of Case Western Reserve University, Boltwood Observatory, the ESO NTT, the observatories of Torino, Tuorla, Perugia and the University of Florida. We thank Charles Dermer for his comments on the paper. A. E. Wehrle, S. C. Unwin, and W. Xu acknowledge support from the NASA Long Term Space Astrophysics Program. E. Pian is grateful for hospitality at IPAC during development of this research and acknowledges support from NASA Long Term Space Astrophysics Program. M. Urry, E. Pian, and J. Pesce acknowledge support from NASA grants NAG8-1037, NAG5-2538, and NAG5-3138. J. Webb acknowledges support from NASA IUE Guest Observer Program. M. F. Aller and H.D. Aller acknowledge support from NSF grant AST-9421979. D. Backman, J. Dalton and G. Aldering were Visiting Astronomers at Cerro Tololo Interamerican Observatory, National Optical Astronomy Observatories, operated by the Association of Universities for Research in Astronomy, Inc. (AURA), under a cooperative agreement with the National Science Foundation. The National Undergraduate Research Observatory (NURO) is operated by Lowell Observatory under an agreement with Northern Arizona University and the NURO

Consortium. The observers from Franklin and Marshall College thank the University of Delaware / Bartol Research Institutes Space Grant Colleges consortium for partial support of NURO membership and observations. The James Clerk Maxwell Telescope is operated by The Joint Astronomy Centre on behalf of the Particle Physics and Astronomy Research Council of the United Kingdom, the Netherlands Organisation for Scientific Research, and the National Research Council of Canada. We thank C. Imhoff, N. Loiseau, and J. Nichols for assistance with IUE observations and data reduction, and E. Solano and W. Wamsteker for timely NEWSIPS reprocessing of part of the IUE spectra.

## REFERENCES

- Barr, P., et al. 1997, in preparation
- Bersanelli, M., Bouchet, P., & Falomo, R. 1991, *A&A*, 252, 854
- Bessel, M. S. 1979, *PASP*, 91, 589
- Blandford, R. D. 1993, in *Compton Gamma-ray Observatory*, AIP Proceedings 280, eds. M. Friedlander, N. Gehrels, and D. J. Macomb (New York: AIP), p. 533
- Cardelli, J. A., Clayton, G. C., & Mathis, J. S. 1989, *ApJ*, 345, 245
- Dermer, C. D., Schlickeiser, R., & Mastichiadis, A. 1992, *A&A*, 256, L27
- Dermer, C. D. 1995, *ApJ*, 446, L63
- Dermer, C. D., & Gehrels, N. 1995, *ApJ*, 447, 103
- Dondi, L., & Ghisellini, G. 1995, *MNRAS*, 273, 583
- Edelson, R. A., & Krolik, J. H. 1988, *ApJ*, 333, 646
- Elvis, M., Lockman, F. J., & Wilkes, B. J. 1989, *AJ*, 97, 777
- Fabian, A. C. 1979, *Proc. Roy. Soc.*, 366, 449
- Falomo, R., Treves, A., Chiappetti, L., Maraschi, L., Pian, E., & Tanzi, E. G. 1993, *ApJ*, 402, 532
- Ghisellini, G., Padovani, P., Celotti, A., & Maraschi, L. 1993, *ApJ*, 407, 65
- Ghisellini, G., & Madau, P. 1996, *MNRAS*, 280, 67
- Ghisellini, G., & Maraschi, L. 1996, in *Blazar Continuum Variability*, ASP Conf. Ser. Vol. 110, Eds. H. R. Miller, J. R. Webb, and J. C. Noble, p. 436
- Hartman, R. C., et al. 1996, *ApJ*, 461, 698
- Hartman, R. C. 1996, in *Blazar Continuum Variability*, ASP Conf. Ser. Vol. 110, Eds. H. R. Miller, J. R. Webb, and J. C. Noble, p. 333
- Hartman, R. C., et al. 1997, in preparation
- Kniffen, D. A., et al. 1993, *ApJ*, 411, 133
- Koratkar, A. P., Pian, E., Urry, C. M., & Pesce, J. E. 1997, *ApJ*, submitted
- Macomb, D. J., et al. 1995, *ApJ*, 449, L99
- Makino, F., Inoue, H., Kii, T., Nagase, F., & Yamashita, A. 1996, *IAU Circ. No.* 6302
- Maraschi, L., Ghisellini, G., & Celotti, A. 1992, *ApJ*, 397, L5
- Maraschi, L., et al. 1994, *ApJ*, 435, L91

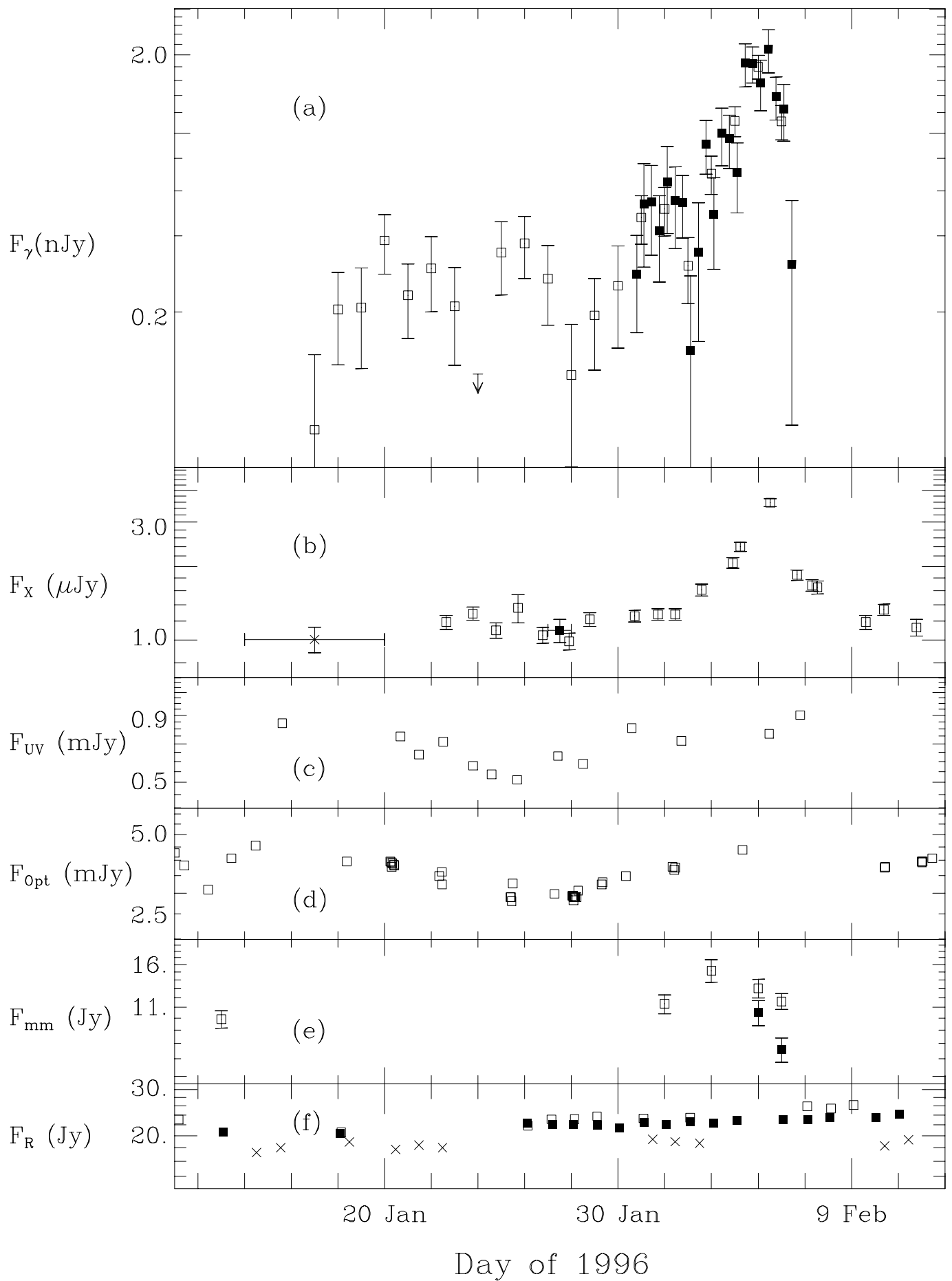
- Marscher, A. P., Marshall, F. E., Mushotzky, R. F., Dent, W. A., Balonek, T. J., & Hartman, M. F. 1979, *ApJ*, 233, 498
- Mattox, J. R., Wagner, S. J., Malkan, M., McGlynn, T. A., Schachter, J. F., Grove, J. E., Johnson, W. N., & Kurfess, J. D. 1997, *ApJ*, 476, 692
- McHardy, I. M., et al. 1997, in preparation
- Nichols, J. S., & Linsky, J. L. 1996, *AJ*, 111, 517
- Pian, E., et al. 1997, in preparation
- Rieke, G. H., & Lebofsky, M. J. 1985, *ApJ*, 288, 618
- Shull, J. M., & Van Steenberg, M. E. 1985, *ApJ*, 294, 599
- Sikora, M., Begelman, M. C., & Rees, M. J. 1994, *ApJ*, 421, 153
- Stoche, J., et al. 1997, in preparation
- Thompson, D. J., et al. 1995, *ApJS*, 101, 259
- Thompson, D. J., et al. 1996, *ApJS*, 107, 227
- Ulrich, M.-H., Maraschi, L., & Urry, C. M. 1997, *ARA&A*, in press
- Urry, C. M., et al. 1997, *ApJ*, submitted
- Webb, J. R., et al. 1996, in Workshop on Two Years of Intensive Monitoring of OJ 287 and 3C 66A, Tuorla Observatory Report N. 176s, Ed. L. O. Takalo, p. 20
- Wehrle, A. E., et al. 1997, in preparation

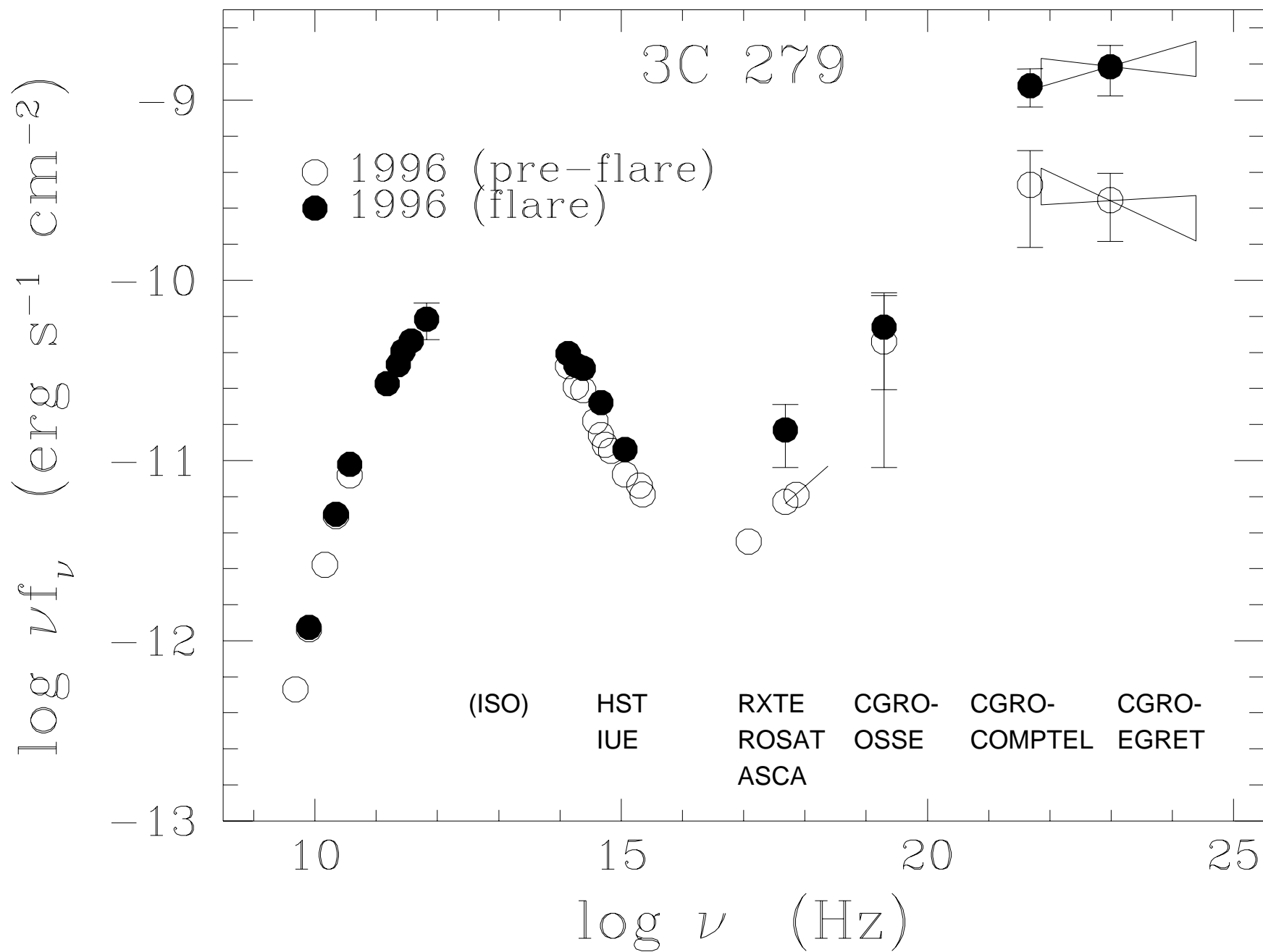
### Figure Captions

Fig. 1.— Multiwavelength light curves of 3C 279 during the EGRET campaign (1996 January 16 - February 6): *(a)* EGRET fluxes at  $>100$  MeV binned within 1 day (open squares) and 8 hours (filled squares) (referred to 400 MeV, following Thompson et al. 1996); *(b)* X-ray fluxes at 2 keV: besides the RXTE data (open squares), the isolated ASCA (filled square) and ROSAT-HRI (cross) points are reported with horizontal bars indicating the total duration of the observation; IUE-LWP fluxes at 2600 Å; *(d)* ground-based optical data from various ground-based telescopes in the R band; *(e)* JCMT photometry at 0.8 mm (open squares) and 0.45 mm (filled squares); *(f)* radio data from Metsähovi at 37 GHz (open squares) and 22 GHz (filled squares), and from UMRAO at 14.5 GHz (crosses). Errors, representing  $1\text{-}\sigma$  uncertainties, have been reported only when they are bigger than the symbol size.

Fig. 2.— Radio-to- $\gamma$ -ray energy distribution of 3C 279 in low (open circles) and flaring state (filled circles) in 1996 January-February. The data plotted correspond to the entries of Table 1, except that the UV, optical and near-IR data have been corrected for Galactic extinction (see text). The slope of the ASCA spectrum ( $\alpha_\nu = 0.7$ ) has been reported normalized to the RXTE point closest in time. The EGRET best fit power-law spectra referring to the January 16-30 (low state) and February 4-6 periods are shown, normalized at 0.4 GeV. Errors have been reported only when they are bigger than the symbol size.

Fig. 3.— Same as in Fig. 2. For comparison, the SEDs in 1991 June (stars) and in 1992 December - 93 January (diamonds) are also shown (see Maraschi et al. 1994). Errors have been reported only when they are bigger than the symbol size.







**Table 1:** Journal of 1996 Multiwavelength Observations of 3C 279

Instrument	Band	Observer (PI)	$\log \nu$ (Hz)	Dates (January)	$\log \langle f_{min} \rangle^a$ ( $\text{erg s}^{-1} \text{cm}^{-2} \text{Hz}^{-1}$ )	Dates (February)	$\log \langle f_{max} \rangle^a$ ( $\text{erg s}^{-1} \text{cm}^{-2} \text{Hz}^{-1}$ )
CGRO/EGRET	30-10000 MeV	Hartman and Wehrle	22.98	25-28	$-32.54^{+0.15}_{-0.23}$ (4)	4.1-5.7	$-31.80^{+0.12}_{-0.16}$ (6)
CGRO/Comptel	10-30 MeV	Collmar	21.68	16-30	$-31.15^{+0.19}_{-0.34}$	1-6	$-30.60^{+0.09}_{-0.12}$
CGRO/OSSE	50-150 keV	McNaron-Brown	19.29	24-27	$-29.63^{+0.26}_{-0.70}$ (4)	3-6	$-29.55^{+0.19}_{-0.35}$ (4)
ASCA	2-10 keV	Makino	17.86 <sup>b</sup>	27.5	$-29.05 \pm 0.05$ (1)	–	–
RXTE	1-10 keV	McHardy	17.68 <sup>b</sup>	24.8-27.9	$-28.91 \pm 0.06$ (4)	4.2-5.5	$-28.51^{+0.14}_{-0.21}$ (2)
ROSAT/HRI	0.1-2.4 keV	Madejski	17.08 <sup>b</sup>	17	$-28.53 \pm 0.05$ (1)	–	–
HST/FOS	1300-2240 Å	Stoche	15.35	8	$-26.59 \pm 0.01$ (1)	–	–
IUE/SWP	1400-1600 Å	Ghisellini and Webb	15.30	25.4	$-26.58 \pm 0.04$ (1)	–	–
IUE/LWP	2500-2700 Å	"	15.06	24.6-27.4	$-26.25 \pm 0.05$ (3)	5.4	$-26.12 \pm 0.02$ (1)
Optical Photometry from Ground-based Telescopes	B V R I	see Table 2 " " "	14.83 14.74 14.67 14.58	28 25.4-28 25.4-28 25.4	$-25.85 \pm 0.02$ (1) $-25.70 \pm 0.02$ (7) $-25.57 \pm 0.02$ (8) $-25.39 \pm 0.03$ (5)	– – 4.3 –	– – $-25.40 \pm 0.02$ (1) –
CTIO (1.5m+NIC)	J H K	Backman " "	14.38 14.26 14.13	31 31 31	$-25.00 \pm 0.01$ (1) $-24.86 \pm 0.041$ (1) $-24.61 \pm 0.021$ (1)	3 3 3	$-24.903 \pm 0.006$ (1) $-24.74 \pm 0.01$ (1) $-24.556 \pm 0.007$ (1)
JCMT	0.45 mm 0.8 mm 1.1 mm 1.3 mm 2 mm	Stevens " " " "	11.82 11.57 11.44 11.36 11.18	– – – – –	– – – – –	5-6 5-6 5-6 5-6 5-6	$-22.04^{+0.09}_{-0.11}$ (2) $-21.91 \pm 0.04$ (2) $-21.83 \pm 0.03$ (2) $-21.83 \pm 0.06$ (2) $-21.75 \pm 0.04$ (2)
IRAM	250 GHz	Freudling	11.40	13	$-21.58^{+0.12}_{-0.16}$ (2)	–	–
Metsähovi Station	37 GHz 22 GHz	Teräsraanta "	10.57 10.34	26-27 26-27	$-21.65 \pm 0.02$ (2) $-21.65 \pm 0.01$ (2)	7 4-6	$-21.59 \pm 0.01$ (1) $-21.64 \pm 0.01$ (2)
UMRAO	14.5 GHz 8 GHz 4.8 GHz	Aller, M. and Aller, H. " "	10.16 9.90 9.68	22.5 28.4 25.4-26.4	$-21.743 \pm 0.006$ (2) $-21.838 \pm 0.007$ (1) $-21.945 \pm 0.005$ (2)	– 4.4 –	– $-21.829 \pm 0.004$ (1) –

<sup>a</sup> Fluxes in the low and flaring state were obtained by averaging the data in the intervals designated in the respective preceding columns.

The number of averaged data points is reported in parentheses. Uncertainties represent standard deviations from the mean values. If only one observation is available, or if the dispersion is less than the typical intrinsic error, the latter is given.

<sup>b</sup> For ASCA, RXTE, and ROSAT/HRI, the frequencies listed correspond to 3, 2, and 0.5 keV, respectively.

**Table 2:** Optical Photometric Monitoring of 3C 279 in 1996: Observers and Instruments

Observer	Observatory	Telescope	Filters	Dates
Aldering	CTIO	0.9m	BRI	27-29 Jan
Backman	NURO, Lowell	0.8m	BVRI	12 Jan
Balonek	Foggy Bottom	16''	VR	18 Jan - 22 Apr
	Case Western Reserve Univ.	Burrell Schmidt	R	8-14 Jan
Boltwood	Boltwood	18cm	VRI	20 Jan - 10 Mar
Falomo	ESO	NTT	V	18.1 Jan
Ghisellini & Villata	Torino	REOSC 1.05m	BVR	4 Jan - 7 Apr
Hall	Steward	90''	griz (Gunn)	28,30 Jan
Kidger & Gonzalez-Perez	Tenerife	82cm	BVR	7,10 Jan
Nair	Univ. of Florida	30''	VR	19 Feb
Takalo & Sillanpää	Tuorla	1.03m	BVR	26 Jan - 12 Feb
Smith	Steward	90''	V	27 Jan
Tosti	Perugia	0.4m	VRI	23 Feb - 20 May